ELSEVIER

Chemical Engineering Journal 68 (1997) 145–155

Chemical Engineering Journal

The effects of a variety of wall obstructions on local mass transfer in a parallel plate electrochemical flow cell

C.F. Oduoza *, A.A. Wragg, M.A. Patrick

School of Engineering, Exeter University, Exeter, EX4 4QF, UK

Received 13 November 1996; revised 19 June 1997; accepted 26 June 1997

Abstract

This paper demonstrates the effects on local mass transfer of placing a variety of partial obstructions in the form of fences or steps (arranged in single or multiple configurations) on the walls of a parallel plate electrochemical flow cell. For the wall on which the fence is placed, a plot of the position of mass transfer relative to an obstruction against the Reynolds number for different fence heights shows that, for each fence, the distance to peak position initially increases with the Reynolds number, but tends to decrease at higher Reynolds numbers. For the wall opposite to the fence, a pronounced peak immediately opposite the obstruction, corresponding to a position of maximum velocity, and a second downstream peak, corresponding to a recirculation/reattachment zone, were identified. A correlation of the peak Sherwood number as a function of the Peclet number for all fence heights and also for a backward-facing step was compared with data of other workers. The numerical prediction of flow reattachment to the walls produced excellent agreement with the positions of peak mass transfer for both the fences and the step, but agreed less well in terms of magnitude. © 1997 Elsevier Science S.A.

Keywords: Local mass transfer; Parallel plate electrochemical flow cell; Wall obstructions

1. Introduction

A sudden change of wall orientation in flow passages significantly affects the characteristics of the flow near the wall and sometimes causes flow separation and reattachment. A typical case is flow over a stepped wall where a forward-facing step forms a sudden compression of the flow, whereas a backward-facing step forms a sudden expansion of the flow. A combination of these two geometries yields either a fence or an open cavity. Flow separation and reattachment are of great importance in fields such as aeronautical, mechanical, civil and chemical engineering and in the environment, because their frequent occurrence may affect fundamental flow characteristics and result in a drastic change in the performance of fluid machinery and heat transfer devices. It is particularly important that modern computational fluid dynamics codes be tested and verified in flow problems with separation and reattachment characteristics.

An abrupt enlargement of the cross-section of a tube or duct creates a downstream zone of flow separation. Beyond the separation zone, the flow reattaches to the duct wall and then redevelops. Experiments involving rectangular ducts [1] have dealt with two-dimensional enlargements where there is a backward-facing step at each of the walls where the enlargement takes place. Sobey [2] has observed steady and oscillatory flow through a two-dimensional channel expansion in both asymmetric and symmetric channels. The experimental results are supported by numerical solutions of the unsteady Navier–Stokes equations. Kim et al. [3] carried out heat transfer measurements in separated, reattached and redeveloped regions of turbulent air flow over a normal fence attached to one surface of a two-dimensional duct. Runchall [4], in an earlier study, reported the results of an experimental investigation which employed the diffusion-controlled electrolysis technique for the determination of mass transfer rates within a wide range of Schmidt and Reynolds numbers in the separated and redevelopment regions downstream of a sudden enlargement of a circular pipe. In separate work, Chouikhi et al. [5] studied local mass transfer rates at the wall of a pipe downstream of a constricting nozzle in turbulent pipe flow at various Schmidt numbers. Effective installation of turbulence promoters for heat transfer augmentation in a vertical rib-heated channel was demonstrated by Hung and Lin [6]. Their results showed that the installation of turbulence promoters in the vertical rib-heated channel can effectively enhance all the rib heat transfer performances in the channel and avoid hot spots occurring in the "quasi equilibrium"

* Corresponding author. Tel.: 00 44 01392 263649; fax: 00 44 01392 217965.

PII S1385-8947(97)00072-7

high temperature regime. Nusselt numbers and the coefficient of channel pressure drop increased with increasing ratio of promoter height to channel spacing. Krall and Sparrow [7] have shown the effect of an orifice situated at the inlet of an electrically heated circular tube on heat transfer in the separated, reattachment and redevelopment regions. Heat and mass transfer enhancement downstream of abrupt nozzle expansions in turbulent flow was demonstrated by Tagg et al. [8]. Using the Chilton–Colburn analogy, the data for the peak mass transfer rate were shown to be correlated well with the independently generated heat transfer data of Krall and Sparrow [7].

The above investigations have demonstrated rapid changes in heat and mass transfer rate and friction coefficient near obstructions, such as fences, ribs or steps, which may provide the potential for the improvement of the design of heat transfer devices, such as cooling systems for electronic components and chemical reactors and cooling passages in turbine blades and combustion chambers.

This work is part of a broader study of industrial electroplating equipment involving complex geometries and complex flows. A long vertical parallel plate flow cell has been set up, whose performance is to be matched against numerically derived data as a check on the validity and accuracy of parallel boundary and finite element modelling approaches by other groups. A relatively simple perturbation to flow is being used as the test case with special focus on the laminar region. The work employs the well-known limiting diffusion current technique of mass transfer measurement [4,5,8,9] in a vertically oriented parallel plate cell.

2. Experimental details

Fence-type obstructions of various heights (3, 5 and 7.5 mm), each 2 mm thick, were positioned on both the test cathode and on the opposite anode wall of a vertical parallel plate cell, and the resulting mass transfer controlled limiting current distributions at the walls were measured. The cell had a total height of 2.210 m, with an inlet section length of 1.03 m and an exit section length of 0.34 m. The working electrode (cathode) was a nickel plate (length, 0.35 m; width, 0.1 m), set in one wall of the channel, and the anode was a nickel plate (length, 0.41 m), set on the opposite wall, with an interelectrode spacing of 0.01 m. The cathode was equipped with 48×1 mm diameter surface flush nickel mini-electrodes arranged in two axially oriented rows in the middle of the plate (16 upstream of the fence and 32 immediately downstream of the fence). In the first series of experiments, the fence was positioned 0.01 m from the leading edge of the cathode, whereas, in the second series, the position of the fence on the anode corresponded to a distance of 0.01 m from the leading edge of the cathode plate. For a third set of experiments involving double fences, the positions of the fences were 0.1 m and 0.2 m respectively from the leading edge of the cathode.

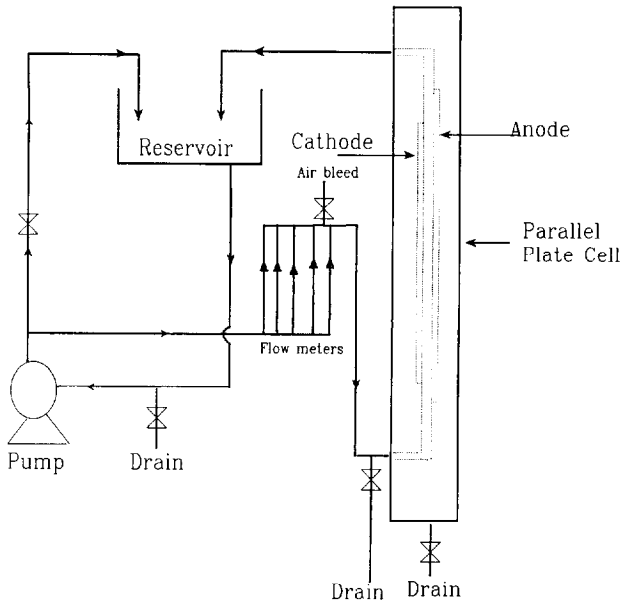

Fig. 1. Schematic representation of the flow rig.

Measurements of local mass transfer downstream of a backward-facing step were carried out by equipping the cell with a PVC block (thickness, 5 mm; width, 10 mm; length, 200 mm) positioned immediately upstream of the macrocathode. The step had a 17° chamfer at the upstream edge of the block. In this case, the entire cathode plate with all of its mini-electrodes lay downstream of the step.

Fig. 1 shows a schematic representation of the flow rig carrying the parallel plate cell, and a diagrammatic plan view of the cathode plate is shown in Fig. 2. Elevations of the cell showing the fence and the backward-facing step are given in Fig. 3(a) and Fig. 3(b) respectively. Fig. 4 shows the relationship between the geometry of the fence and the channel. The assembly of the nickel mini-electrodes on the nickel macroelectrode was tedious, and was performed carefully using Araldite 2004 to secure them in position, whilst ensuring complete electrical insulation from the macrocathode.

The data acquisition system was made up of an Elonex (IBM-compatible) computer, a microcontroller subsystem containing 64 operational amplifiers and a 16 bit analogue to digital (A to D) converter and multiplexer. Electrical power to the cell was partly supplied by a Thurlby power supply (PL 154) and Thandar TS 3023S dual channel precision d.c. power supply, which powered the operational amplifiers controlling the output from the mini-electrodes. The d.c. output from the macroelectrode was monitored through a Thurlby Thandar 1906 computing multimeter with autoranging facilities, but outputs from the mini-electrodes were converted to voltage, and then multiplexed to a 16 bit A to D converter. The microcontroller then buffered and relayed the digitized information to the computer for display. Twenty measurements were made on each mini-electrode at a sampling frequency of 10 Hz, and the average measurement was displayed as a histogram.

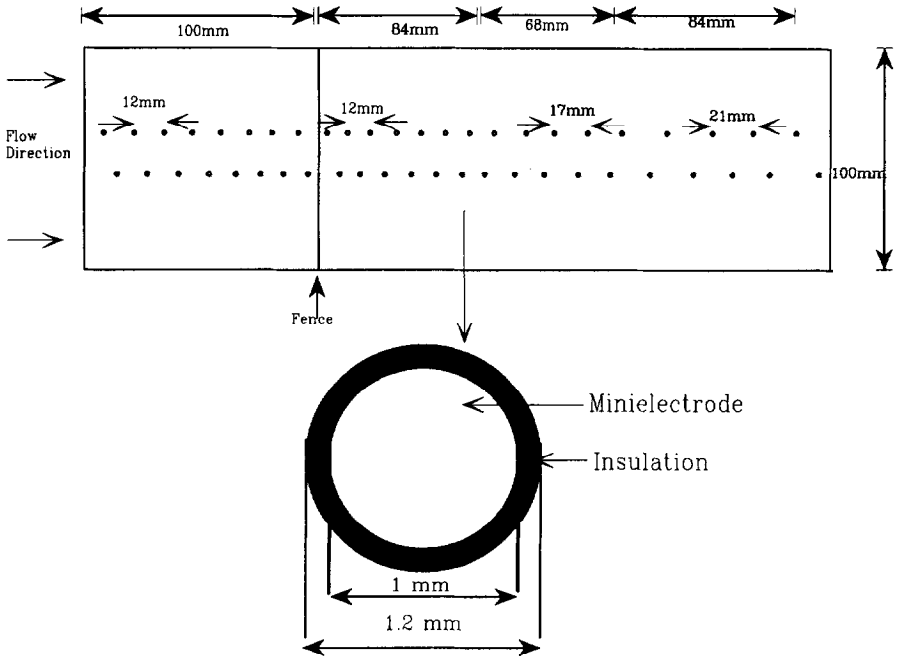

Fig. 2. Cathode showing disposition of microelectrodes.

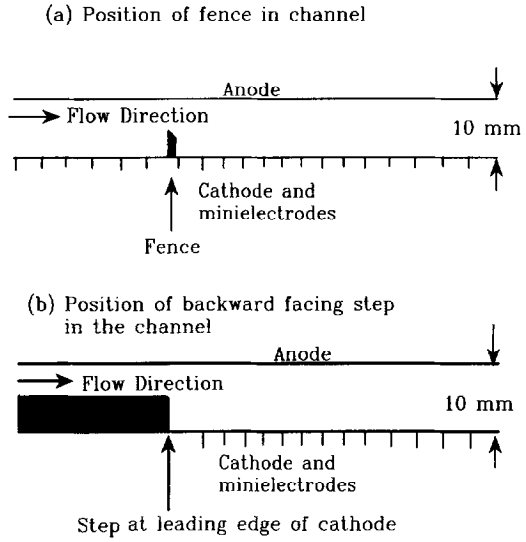

Fig. 3. (a) Position of fences in the parallel walled channel. (b) Position of backward-facing step in the parallel walled channel.

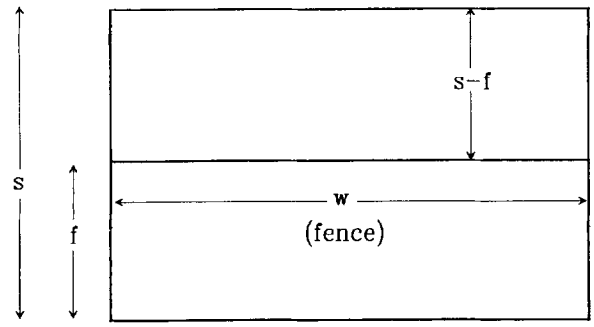

Fig. 4. Relationship between the fence and the channel.

The potassium ferrocyanide (0.01 M)/ferricyanide (0.005 M)/sodium hydroxide (0.5 M)/water system was used as electrolyte, and local limiting currents were measured for the cathodic reduction of ferricyanide ion to ferrocyanide ion

$$Fe(CN)_6^{3-} + e \rightarrow Fe(CN)_6^{4-}$$

The physical properties of the electrolyte at 20 °C [9] are listed in Table 1.

Before each experiment, the cathode surface was cleaned and polished using different grades of wet or dry paper. Voltage was then applied beyond the limiting current region of 1.2 V for about 5 min to liberate hydrogen. This had the effect of removing surface oxides. By applying a potential of 800 mV between anode and macrocathodes, i.e. the mid-plateau region of the current–potential curves, limiting current values for each mini-electrode for a range of Reynolds numbers were determined. Local mass transfer coefficients were then calculated using the equation

Table 1
Physical properties of the electrolyte at 20 °C [8]

Concentration of $K_3Fe(CN)_6$ (potassium ferricyanide)	0.005 M
Concentration of $K_4Fe(CN)_6$ (potassium ferrocyanide)	0.01 M
Concentration of NaOH (sodium hydroxide)	0.5 M
Density	1020.5 kg m^{-3}
Viscosity	1.105×10^{-3} kg m^{-1} s^{-1}
Diffusivity of ferricyanide ion	6.631×10^{-10} m^2 s^{-1}
Schmidt number	1633

$$K_m = \frac{I_{lim}}{zFAC} \quad (1)$$

where I_{lim} is the mini-electrode limiting current, z is the number of electrons exchanged ($z=1$), F is the Faraday number (96 487 C mol^{-1}), A is the exposed mini-electrode area (7.85×10^{-7} m^2) and C is the bulk $Fe(CN)_6^{3-}$ concentration.

The temperature was maintained at 20 °C using a water-cooled heat exchanger in the electrolyte reservoir, oxygen was removed from the electrolyte by nitrogen bubbling and the ferricyanide concentration was periodically determined using UV spectrophotometry.

Data from the mini-electrodes were collected and processed using the data acquisition system described above. The raw and average data values for each mini-electrode were saved to disk and accessed and processed off-line.

3. Results and discussion

3.1. Single fence obstruction

The mass transfer coefficient distributions at different jet Reynolds numbers for a 7.5 mm fence are shown in Fig. 5. The jet Reynolds number was calculated on the basis of the jet velocity. The fence causes a peak in mass transfer immediately downstream, followed by a gradual trend towards the fully developed downstream value. Fig. 6 shows a plot of the magnitude of the peak value of K against jet Re. K increases with Re and with the size of the fence. This is a similar finding to that of Sparrow and Kalejs [1] and Kim et al. [3]. A larger fence height produces a stronger jetting effect for a constant duct-based flow rate, thus yielding a higher mass transfer peak. A plot of peak position, relative to the fence, against Reynolds number for different fence heights is shown in Fig. 7. For each fence height, the peak position initially increases with the Reynolds number, but then tends to decrease at higher Reynolds numbers. This trend in peak position can be clearly discerned from the distributions plotted in Fig. 5. A log plot of Sherwood number (peak)/$Sc^{0.33}$ against the jet Reynolds number, averaged over three experiments, is shown in Fig. 8. Here the Sherwood number is based on the jet equivalent diameter. This plot achieves a successful correlation of the data for all the fences. The equation through the points is $Sh=0.137Re^{0.67}Sc^{0.33}$. The

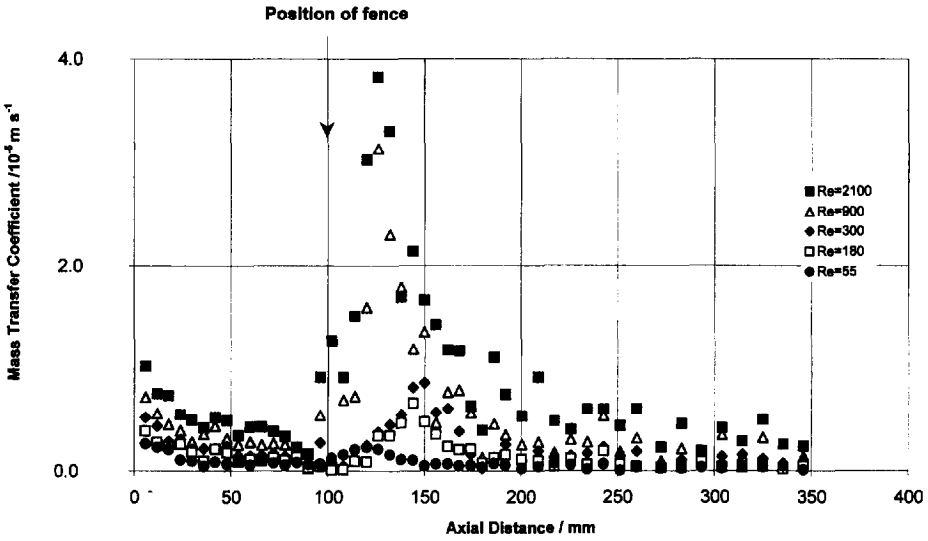

Fig. 5. Effect of fence, 7.5 mm in height, on the mass transfer coefficient distributions at different Reynolds numbers.

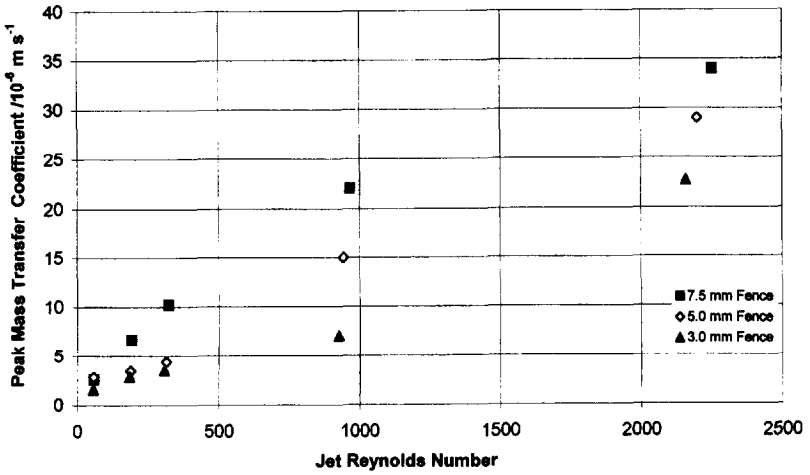

Fig. 6. Peak mass transfer coefficient against Reynolds number for different fence heights.

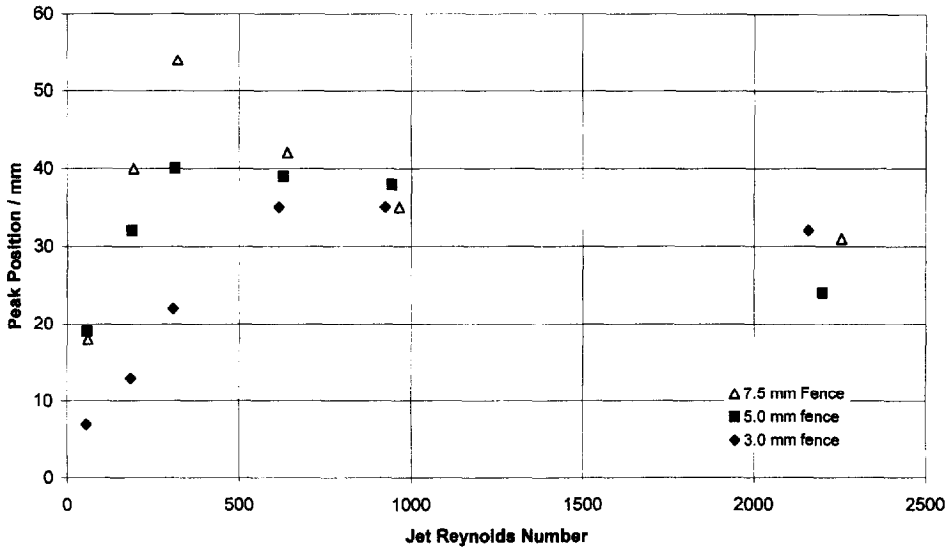

Fig. 7. Peak position relative to fence against Reynolds number for different fence heights.

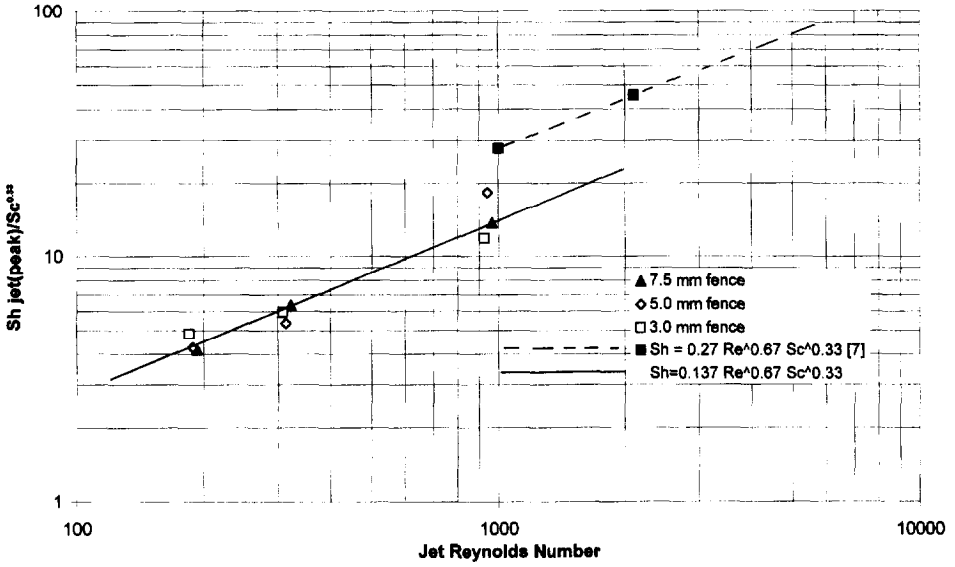

Fig. 8. Log scale plot of Sh_{jet} (peak) / $Sc^{0.33}$ against Reynolds number at the cathode.

correlation of Tagg et al. [8] in turbulent flow with an axisymmetrical cell is also shown in this plot ($Sh = 0.27Re^{0.67}Sc^{0.33}$), and is seen to lie consistently higher than the present laminar flow data.

3.2. Opposite wall fence obstruction

Fig. 9(a) shows the effect of the 7.5 mm obstruction positioned on the opposite wall on the local mass transfer at the cathode for Reynolds numbers of 400 and 600. The plots are characterized by three distinct features at all Reynolds numbers:

1. the decay of the mass transfer coefficient from the leading edge of the cathode plate;
2. a pronounced peak immediately opposite the fence obstruction corresponding to the position of maximum mean velocity;
3. a second downstream peak corresponding to a recirculation zone on the opposite wall from the obstruction.

Fig. 9(b) shows the K distribution for the higher Reynolds number of 900, where the two peaks visible in Fig. 9(a) have merged into a single large peak. There is also some waviness in the far downstream data due to a possible further weak recirculation zone in that region. For the different fences, a comparatively higher fence produces a higher velocity at the plane of obstruction and therefore a proportionately higher mass transfer rate. The same trend was observed for both the first and second peak mass transfer coefficients for the different fences. Generally, it was also observed that the first

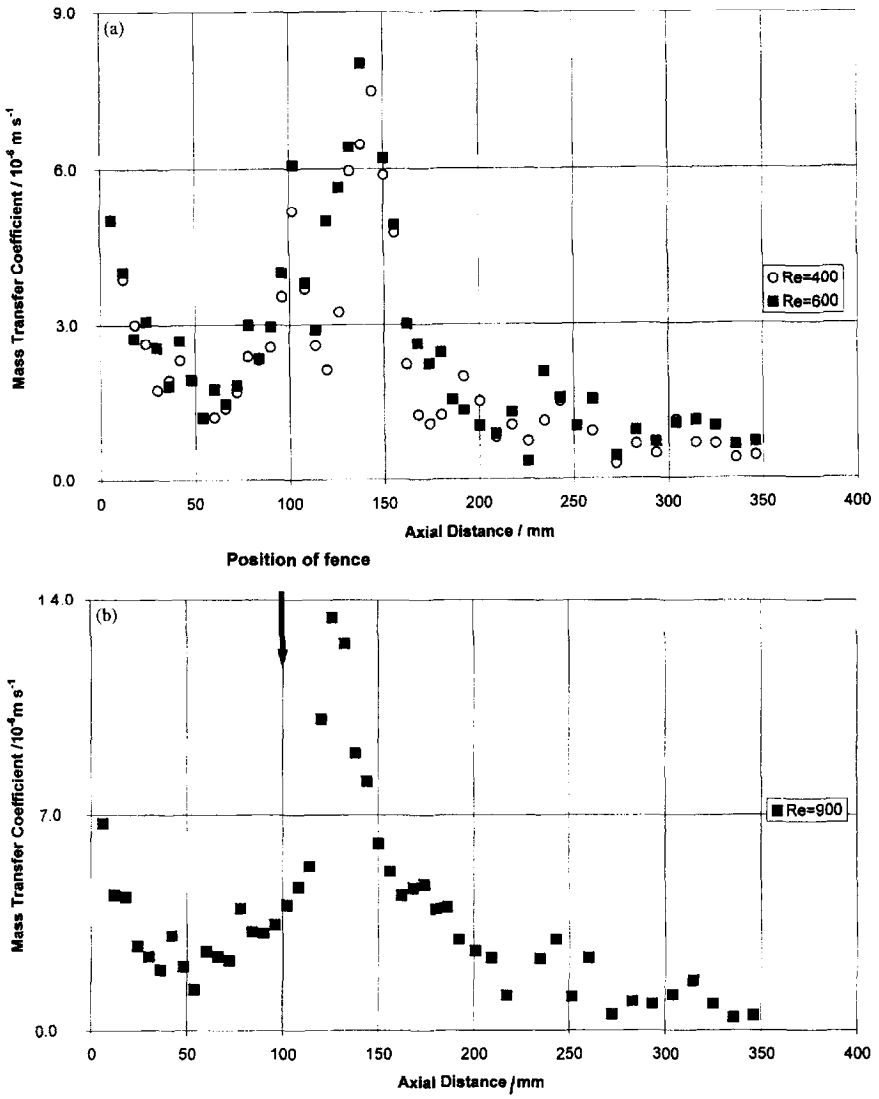

Fig. 9. (a) Effect of 7.5 mm fence on the opposite wall on the mass transfer coefficient distribution at Reynolds numbers 400 (0.023 m s^{-1}) and 600 (0.033 m s^{-1}) (fence at 100 mm). (b) Effect of 7.5 mm fence on the opposite wall on the mass transfer coefficient distribution at a Reynolds number of 900 (0.05 m s^{-1}) (fence at 100 mm).

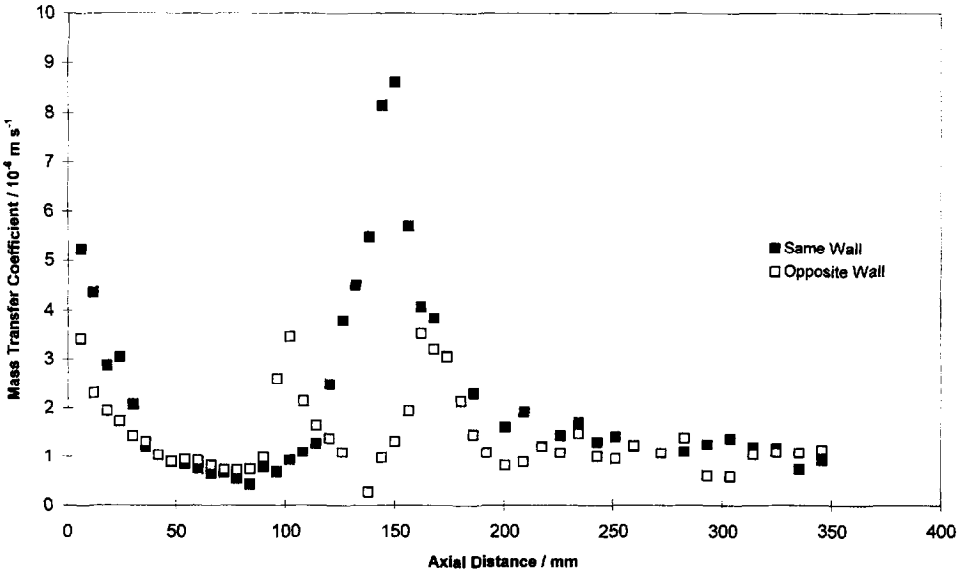

Fig. 10. Comparison of the mass transfer coefficient for a 7.5 mm obstruction on both walls at a Reynolds number of 300 (0.0165 m s^{-1}).

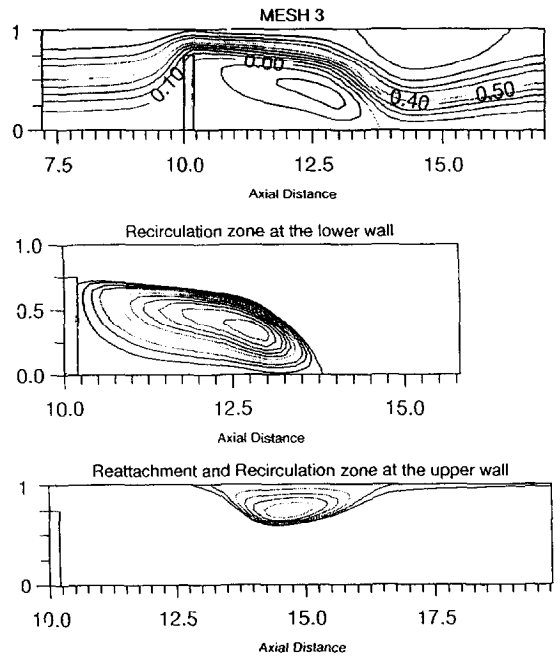

Fig. 11. Flow modelling for a Reynolds number of 100 (0.0055 m s^{-1}) for the recirculation zone at the lower wall and for the reattachment and recirculation zones at the upper wall with a fence height of 7.5 mm.

peak positions remained opposite the fence for all fence heights and Reynolds numbers, whereas there was a change in position of the second peak for all fence heights and Reynolds numbers.

In Fig. 10, a comparison is made of the mass transfer data for the obstruction positioned on each wall. For a fence height of 7.5 mm and Reynolds number of 300, the peak for the "same wall" obstruction lies between the two peaks obtained with the obstruction on the opposite wall. The single peak is comparatively higher than each of the two peaks in the opposite wall situation in all cases. The observed behaviour is consistent with the flow patterns predicted by finite element modelling work [10], as shown in Fig. 11 for a Reynolds number of 100. The existence of recirculation "bubbles" downstream of the fence and also on the upper wall of the duct is clear.

3.3. Double fence obstructions

Fig. 12 shows the effect of double fence obstructions on the mass transfer in the test cell for the 7.5 mm fence height and Reynolds numbers of 55 to 300. There is a disturbance to flow produced by the first obstruction, which results in flow separation, an increased flow velocity due to the constriction and an area of increased mass transfer downstream of the fence. Subsequently, there is a further flow disruption caused by the second fence and a repetition of the trend as for the first fence. The peak magnitude and positions in all cases studied were a function of the fence size and flow velocity. It was also notable in the case of double obstructions that, as Re increases, the first fence to peak distance becomes shorter than the second due to the fact that the recirculation zone following the first fence is restricted in length by the presence of the second fence. Fig. 13 shows a plot of the distance of the first fence to the first peak compared with the second fence to the second peak. A comparison of the peak height and distances with single fences shows that, while the magnitudes of the peaks are identical, the position of the peak in a single fence is further downstream of the fence compared with the first fence in a double obstruction. This situation is consistent at all the flow velocities investigated.

3.4. Backward-facing step

Fig. 14 shows the axial mass transfer distributions at different Reynolds numbers for the 5 mm backward-facing step. It can be seen that the distance to peak increases with increas-

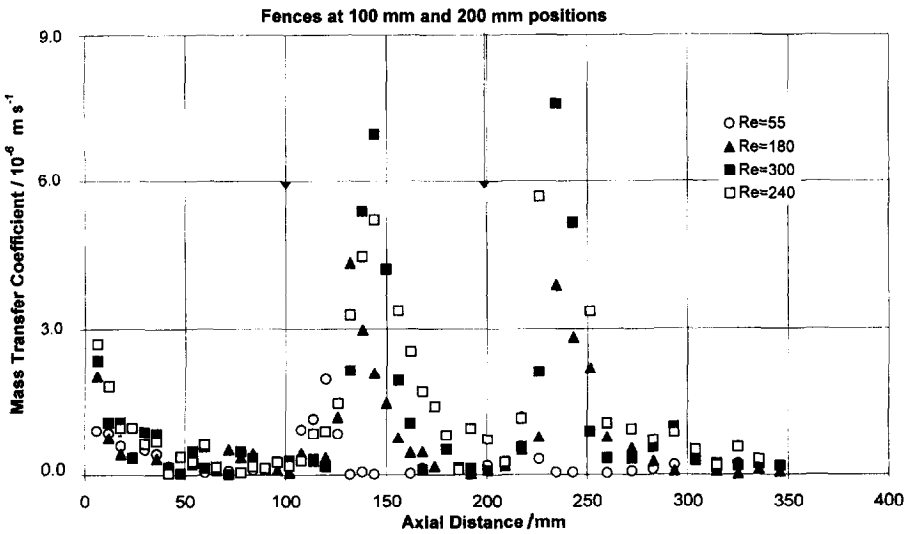

Fig. 12. Effect of two 7.5 mm fences positioned 100 and 200 mm from the leading edge on the mass transfer coefficient distribution at different Reynolds numbers.

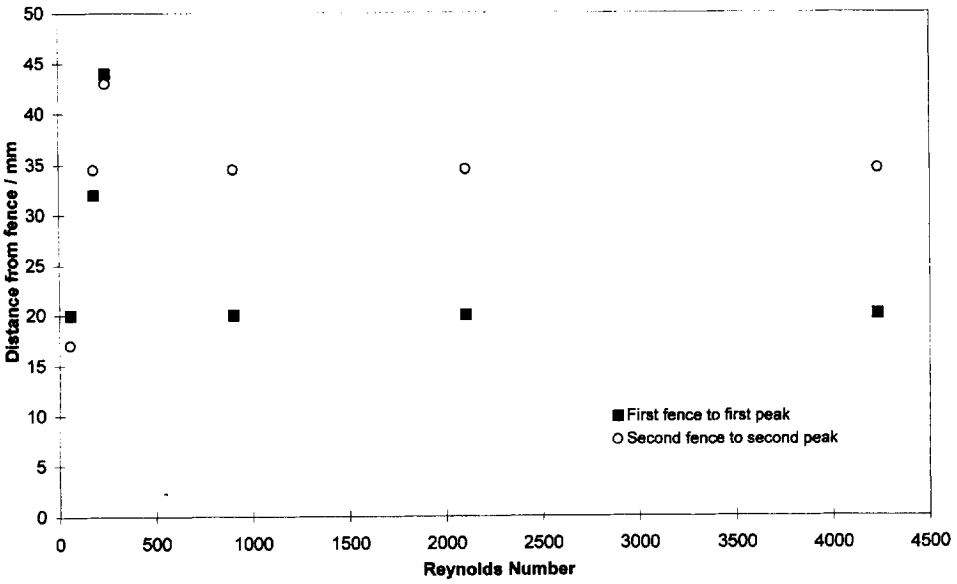

Fig. 13. Plot of the distance of the first fence to first peak compared with the second fence to second peak.

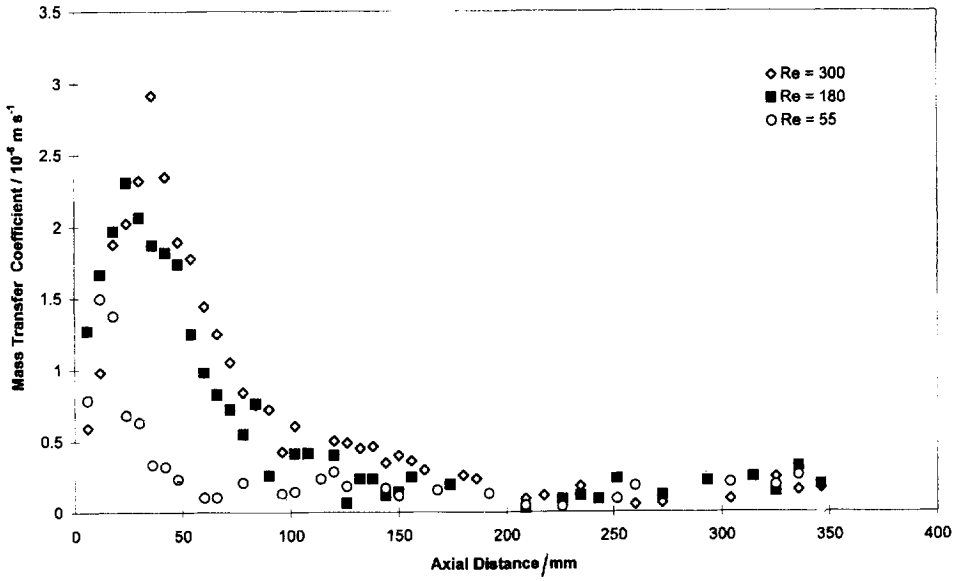

Fig. 14. Effect of 5 mm backward-facing step (immediately upstream of the macrocathode at 0 mm) at Reynolds numbers of 55 (0.0033 m s^{-1}), 180 (0.01 m s^{-1}) and 300 (0.0165 m s^{-1}).

ing Reynolds number. A comparison of the peak K magnitude and distance to peak data for the step with the same values for the 5 mm fence is shown in Fig. 15 and Fig. 16. At low Reynolds numbers, there is a particularly close agreement between the results for the two geometries. At higher Reynolds numbers, the fence to peak position distance becomes distinctly shorter than the step to peak position distance at lower Reynolds numbers. Fig. 17 shows a comparison of the experimental peak Sherwood number as a function of Re with the finite element model for a 5 mm fence [11]. The finite element analysis only applies in the laminar flow region. A close agreement is obtained at low Reynolds numbers. Bogaerts et al. [12] have calculated the positions of peak K using finite element methods (downstream of the 5 mm backward-facing step and the 5 mm fence for Reynolds numbers of 300 and below). Fig. 18 shows a comparison of their predictions with the present experimental data for the 5 mm fence. Again, there is excellent agreement between the finite element model and the experimental data at low Reynolds numbers. Good agreement was also found for the backward-facing step. However, at higher Reynolds numbers, the model begins to fail because of the onset of unsteady flow, and therefore comparison cannot be made with the experimental data in this region. Sparrow et al. [13] have reported the

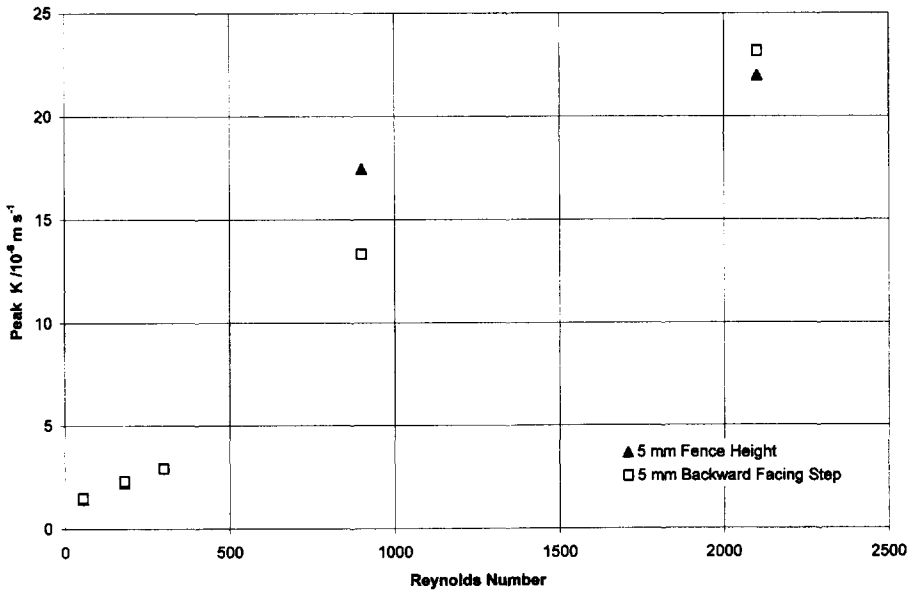

Fig. 15. Comparison of the peak mass transfer coefficient against Reynolds number for a 5 mm backward-facing step and a 5 mm fence height.

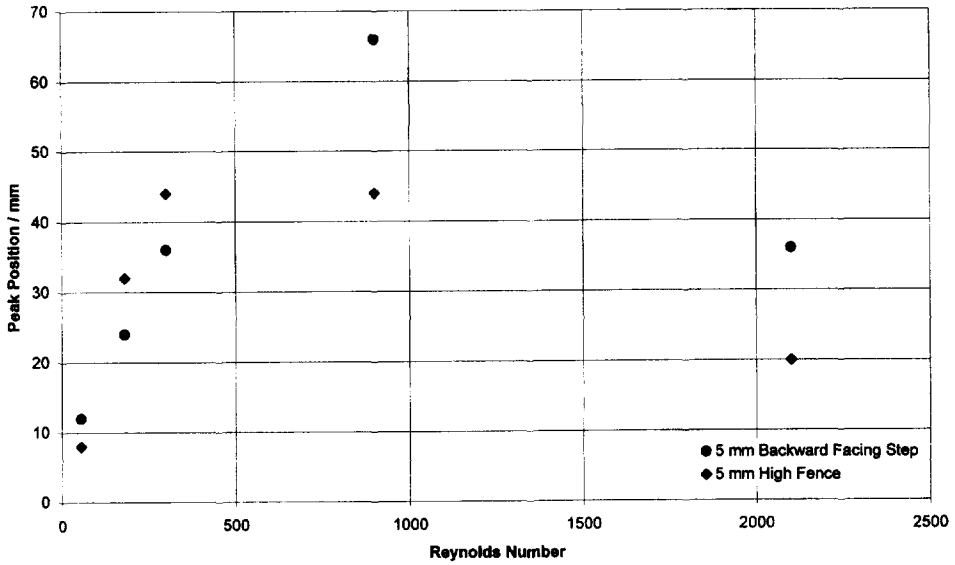

Fig. 16. Comparison of the peak position against Reynolds number for a 5 mm backward-facing step and a 5 mm fence height.

relationship between the reattachment length and the location of the maximum heat transfer rate for laminar flow in a channel with a backward-facing step, using the vorticity–stream function approach. Their results show that the commonly reported correspondence of the points of flow reattachment and maximum heat transfer is not perfectly correct; rather, for most cases, the heat transfer maximum occurs upstream of the reattachment point. Armaly et al. [14], in describing their laser Doppler measurements of velocity distribution and reattachment lengths for a backward-facing step, concluded that the various flow regimes investigated are characterized by the variation of the separation length with the Reynolds number.

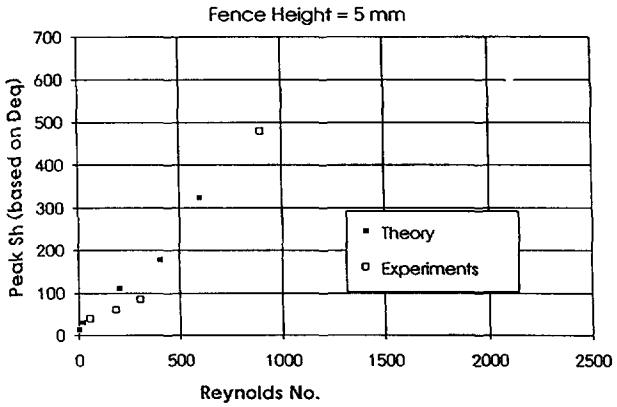

Fig. 17. Comparison of the experimental peak Sherwood number distribution with the finite element model for a 5 mm fence.

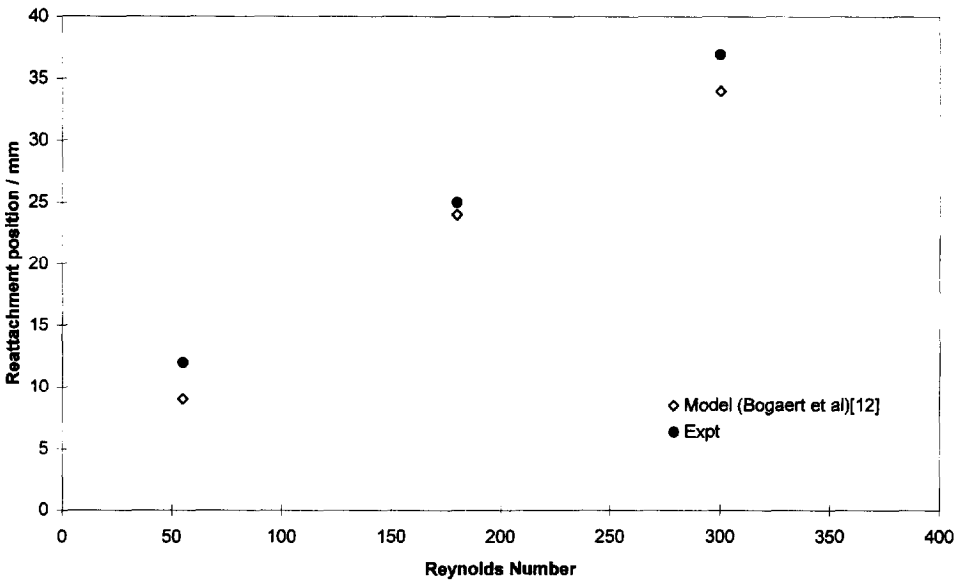

Fig. 18. Positions of reattachment downstream of a 5 mm fence on the cathode.

4. Conclusions

This paper has investigated the effects of a variety of wall obstructions on a parallel plate electrochemical cell. Experimental and numerical results show that the mass transfer rate depends on the type and size of obstruction, and its position in the flow channel. A large fence height produces a stronger jetting effect for a constant duct-based flow rate, thus yielding a higher mass transfer peak, compared with a small fence. The position of peak mass transfer downstream of a fence or step is dependent on the Reynolds number, and lies between the flow recirculation and reattachment zones. For each fence height, the peak position initially increases with Reynolds number, but then decreases at higher Reynolds numbers. This observation has been confirmed by other workers [8,12].

Acknowledgements

This work was supported within the BRITE Euram programme of the European Commission (project number BE-5187).

Appendix A. Nomenclature

A	electrode surface area (m^2)
C	bulk species concentration (mol m^{-3})
D	diffusion coefficient ($m^2\ s^{-1}$)
d_{ed}	duct equivalent diameter $[4(ws)]/[2(w+s)]$ (m)
d_{ej}	jet equivalent diameter $\{4[w(s-f)]\}/\{2[w+(s-f)]\}$ (m)
F	Faraday constant (96 487 C mol^{-1})
f	fence height (mm)
i_L	limiting electrolysis current (A)
K	mass transfer coefficient ($m\ s^{-1}$)
L	electrode length (m)
Pe	Peclet number (Re × Sc)
Q	volumetric flow rate in duct ($m^3\ s^{-1}$)
Re_d	Reynolds number (duct) $(d_{ed}v_d\rho/\mu)$
Re_j	Reynolds number (jet) $(d_{ej}v_j\rho/\mu)$
Sc	Schmidt number (ν/D)
Sh_{de}	Sherwood number based on duct equivalent diameter (Kd_e/D)
Sh_{jet}	Sherwood number based on jet equivalent diameter (Kd_{ej}/D)
s	interelectrode distance (m)
v_d	duct velocity (Q/ws) ($m\ s^{-1}$)
v_j	jet velocity $(Q/w(s-f))$ ($m\ s^{-1}$)
w	electrode width (m)
z	electrons exchanged in electrode reaction
ρ	fluid density ($kg\ m^{-3}$)
ν	kinematic viscosity ($m^2\ s^{-1}$)
μ	dynamic viscosity ($kg\ s^{-1}\ m^{-1}$)

References

[1] E.M. Sparrow, J.P. Kalejs, Int. J. Heat Mass Transfer 20 (1977) 1241–1249.
[2] I.J. Sobey, J. Fluid Mechanics 151 (1985) 395–426.
[3] K.C. Kim, M.K. Chung, Y. Kim, Int. Comm. Heat Mass Transfer 14 (1987) 531–542.
[4] A.K. Runchall, Int. J. Heat Mass Transfer 14 (1971) 781–792.
[5] S.M. Chouikhi, M.A. Patrick, A.A. Wragg, J. Appl. Electrochem. 17 (1987) 1118–1128.

[6] Y.H. Hung, H.H. Lin, Int. J. Heat Mass Transfer 35 (1992) 29–42.
[7] K.M. Krall, E.M. Sparrow, J. Heat Mass Transfer 88 (1966) 131–136.
[8] D.J. Tagg, M.A. Patrick, A.A. Wragg, Trans. IChemE 57 (1979) 176–181.
[9] A.A. Wragg, A.A. Leontaritis, Chem. Eng. J. 66 (1977) 1–10.
[10] F.P. Plachco, M. Lahoubi, M.A. Patrick, University of Exeter Brite Euram Project Report, BE-5187, September, 1993.
[11] C.F. Oduoza, M.A. Patrick, A.A. Wragg, University of Exeter Brite Euram Project Report, BE-5187, October, 1994.
[12] S. Bogaerts, T. De Mulder, P. Vankeirsbilck, VKI Technical Report 3, Brite Euram Project (BE-5187), 1995, p. 66.
[13] E.M. Sparrow, S.S. Kang, W. Chuck, Int. J. Heat Mass Transfer 30 (1987) 1237.
[14] B.F. Armaly, F. Durst, J.C.F. Pereira, B. Schounung, J. Fluid Mechanics 127 (1983) 473.